



HAL
open science

Meta-model-based multi-objective optimization for robust color reproduction using hybrid diffraction gratings

Soukaina Es-Saidi, Sylvain Blaize, Demetrio Macías

► **To cite this version:**

Soukaina Es-Saidi, Sylvain Blaize, Demetrio Macías. Meta-model-based multi-objective optimization for robust color reproduction using hybrid diffraction gratings. *Optics Express*, 2020, 28 (3), pp.3388. 10.1364/OE.28.003388 . hal-02467074

HAL Id: hal-02467074

<https://utt.hal.science/hal-02467074>

Submitted on 4 Feb 2020

HAL is a multi-disciplinary open access archive for the deposit and dissemination of scientific research documents, whether they are published or not. The documents may come from teaching and research institutions in France or abroad, or from public or private research centers.

L'archive ouverte pluridisciplinaire **HAL**, est destinée au dépôt et à la diffusion de documents scientifiques de niveau recherche, publiés ou non, émanant des établissements d'enseignement et de recherche français ou étrangers, des laboratoires publics ou privés.



Meta-model-based multi-objective optimization for robust color reproduction using hybrid diffraction gratings

SOUKAINA ES-SAIDI,^{1,2} SYLVAIN BLAIZE,¹ AND DEMETRIO MACÍAS^{1,*}

¹Charles Delaunay Institute, CNRS FRE 2019, Light, Nanomaterials, Nanotechnologies (L2N), University of Technology of Troyes, 10300 Troyes, France

²SURYS, Parc d'activités Gustave Eiffel, 22 Avenue de l'Europe, 77607 Bussy-Saint-Georges, France

*demetrio.macias@utt.fr

Abstract: We propose an efficient and versatile optimization scheme, based on the combination of multi-objective genetic algorithms and neural-networks, to reproduce specific colors through the optimization of the geometrical parameters of metal-dielectric diffraction gratings. To illustrate and assess the performance of this approach, we tailor the chromatic response of a structure composed of three adjacent hybrid V-groove diffraction gratings. To be close to the experimental situation, we include the feasibility constraints imposed by the fabrication process. The strength of our approach lies in the possibility to simultaneously optimize different contradictory objectives, avoiding time-consuming electromagnetic calculations.

© 2020 Optical Society of America under the terms of the [OSA Open Access Publishing Agreement](#)

1. Introduction

The generation of structural colors using metallic, dielectric or hybrid nanostructures is currently the subject of a significant amount of research works [1–3]. The interest on this mechanism for color generation arises from its great potential for the design of ultra-thin color-tunable devices, with high resolution and efficiency beyond the diffraction limit, for applications in optical security, imaging and display technologies or color filtering [4–6]. Also, structural coloration is an important complement to traditional colorant-based pigmentation mechanisms.

Very often, however, the chromatic response of the structures used for color generation is characterized through parametric studies based on the systematic variation of their different geometrical parameters. Although this approach has proven successful, it can be very time consuming and does not necessarily provide the optimal solutions that best match the searched colors. Several works making use of mono-objective optimization algorithms have been focused on the solution of this kind of inverse problem [7,8]. Nevertheless, when the studied structures are complex it is necessary to satisfy simultaneously several often contradictory objectives. In that case there is not a single optimal solution but multiple trade-off solutions among the searched objectives, making thus necessary to resort to more sophisticated strategies like multi-objective optimization. This approach has been explored by Wiecha et al to design colour pixels based on silicon nano-structures [9] and by J.Jung to simultaneously improve the performance and robustness of a plasmonic wave-guide [10]. However, since several iterations are needed to search for the optimal solutions, one strategy proposed to avoid time-consuming electromagnetic calculations is to replace them with approximations based on meta-models. Meta-Modeling is increasingly used due to the ongoing improvement of high-performance computer systems and particularly the evolution of artificial intelligence tools, which not only have become a powerful method for the modelling of physical phenomena, but also to understand, simulate and predict the optical or resonant response of the interaction between light and matter at the nanoscale [11–16].

In this work, we propose an efficient multi-objective optimization (MOO) scheme, based on the combination of Genetic Algorithms (GA) with a neural-networks-based meta-model, to tailor the chromatic response of hybrid metal-dielectric gratings. We make use of the meta-model to replace the time-consuming electromagnetic method, required to compute the spectral data related to the colors generated with the grating.

This contribution is organized as follows: In Sect. 2 we describe the geometry of the diffraction grating studied throughout this work. Also, we succinctly outline the rigorous electromagnetic method used to generate the spectra from which the colors are generated. Furthermore, we introduce and describe the meta-model used. In Sect. 3, we formulate the inverse problem to be solved and introduce the variables of interest to be optimized together with the constraints to be satisfied. We present our main results in Sect. 4, where we first illustrate the limitations of mono-objective optimization through an example and then we show the optimal solutions obtained with our MOO scheme. Furthermore, through a post-optimization procedure we discuss robustness of the optimal solutions found and their sensitivity to fabrication errors. Also, we study the influence of the grating's geometrical parameters on the colors generated. Finally, in Sect. 5 we present our concluding remarks.

2. Direct problem: meta-model-based generation of spectral data

Throughout this work we consider, without loss of generality, the periodically corrugated hybrid multilayered structure depicted in Fig. 1. The profile $z = s(x)$ is assumed to be invariant along the y direction and is piece-wise defined by Eq. (1) :

$$s(x) = \begin{cases} \frac{2h}{x_2-x_1} \left| x - \frac{x_1+x_2}{2} \right| & \text{if } x \in [x_1, x_2] \\ h & \text{otherwise,} \end{cases} \quad (1)$$

where h is the amplitude of the grating. The aperture of the V-groove region is defined as $R_\alpha = T_\alpha/\Lambda$ with $T_\alpha = |x_2 - x_1|$ and Λ represents the grating's period. The region $s(x) < z < s(x) + e_A$ is filled with a uniform layer of aluminum (Al) whereas the region $s(x) + e_A < z < s(x) + e_S$ is filled with Silicon Nitride (Si_3N_4), a high refractive index material. We denote the Al and Si_3N_4 layers' thicknesses e_A and e_S , respectively.

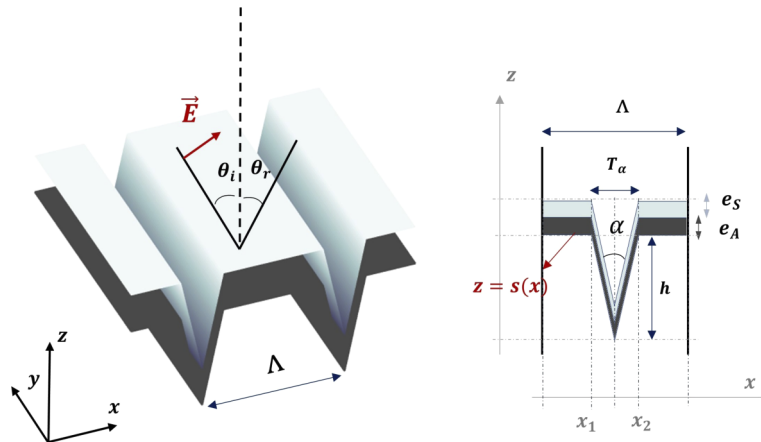


Fig. 1. Geometry of the hybrid metal-dielectric V-groove grating considered in our contribution.

The two semi-infinite regions $z \geq s(x) + e_A + e_S$ and $z \leq s(x)$ are assumed to be isotropic and homogeneous media with refractive indices equal to 1.5. This configuration corresponds to the

case in which the fabricated structure is protected from surrounding wear with a transparent dielectric overlay.

For the sake of brevity, in our study we arbitrarily consider the TM polarization (p-polarization) where the magnetic field is parallel to the V-groove axis (Oy) and we assume that the plane of incidence is the plane (Oxz). Nevertheless, the TE polarization state could be also used.

2.1. C-Method

The theoretical spectral data related to the V-groove grating shown in Fig. 1 are computed using the C-Method, also known as Chandezon Method, through the commercial software McGrating [17]. The C-method is a well known and powerful tool especially suited for the computation of diffraction efficiencies of shallow sinusoidal or pseudo-sinusoidal gratings. It solves Maxwell's equations using the following coordinates transformation [18,19]:

$$\begin{cases} v = x; \\ w = y; \\ u = z - s(x) \end{cases} \quad (2)$$

where $s(x)$ is the grating's profile. Although this transformation complicates the functional form of Maxwell's equations, the surface roughness is flattened, thus making the matching of boundary conditions simpler. In the new (u,v,w) coordinates system, the problem is reduced to an eigenvalues problem whose resolution determines the propagative and evanescent modes of the system.

Unlike other methods [20], it has been shown that the convergence of the C-method depends weakly on the incident field's polarization and material permittivities. Also, it is well suited for multi-layer systems as the one studied in this contribution [21]. However, an important limitation is the aspect ratio and the sharp edges of the profile, which may introduce discontinuities in the profile's derivative function that may generate numerical instabilities in Fourier space.

In our case, to insure fast convergence, to avoid spurious effects and to remove the hyper singularities at the sharp edges [22] (marked with red circles in Fig. 2), we rounded them using a spline function considering a radius of curvature of about 7 nm for the corners and 2 nm for the tip end. These values were selected from convergence and computing time considerations. The grating's profile with rounded edges can be defined by means of a Fourier series. It is noteworthy to mention that in a experimental situation this rounding effect is unavoidable.

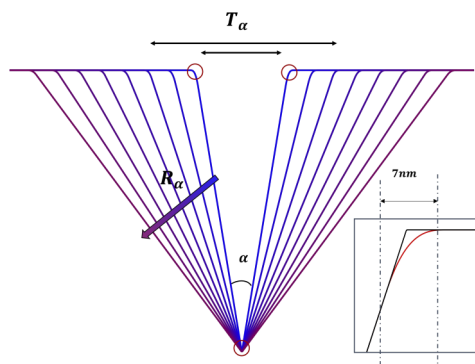


Fig. 2. Variation of the V-groove angle. The insert Fig shows the rounded edges used for better convergence when simulating the structure.

It must be mentioned that depending on the V-groove's depth and aperture it is necessary to readjust the number of harmonics to ensure convergence. As a matter of fact, the smaller the angle, the slower the convergence because the edges are steeper. For this reason, we introduced a convergence loop in our process to generate the reflectance spectra and we set a stop error criterion of 10^{-3} between two consecutive iterations. Figure 3 shows the evolution of the absolute error $|R_{0N} - R_{0N-1}|$ calculated throughout the convergence loop as a function of the number of harmonics. The red line defines the stop criterion. For example, for a V-groove grating defined with $\Lambda = 310\text{nm}$ and $h = 120\text{nm}$, we need 51 harmonics to ensure convergence for the grating with $R_\alpha = 0.6$, against 91 harmonics in the case of $R_\alpha = 0.2$, corresponding respectively to 75.5° and 28.9° V-groove angles.

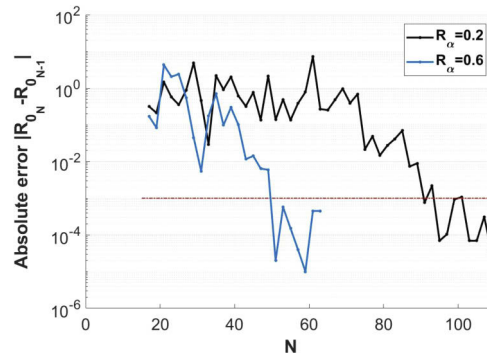


Fig. 3. Evolution of the absolute error calculated throughout the convergence loop as a function of the number of harmonics. The red line defines the error stop criterion of 10^{-3} . For a V-groove grating defined with $\Lambda = 310\text{nm}$ and $h = 120\text{nm}$, we need 51 harmonics to ensure convergence for the one with $R_\alpha = 0.6$, against 91 harmonics in the case of $R_\alpha = 0.2$, corresponding respectively to 75.5° and 28.9° V-groove angles.

2.2. Meta-model

To better understand how the meta-model is used in this work, let us consider two sets X and Y of N elements x_i and y_i $i \in [1 \dots N]$, respectively. Each element x_i can be interpreted as a vector whose components are the geometrical parameters $(R_\alpha, \Lambda, h, e_A, e_S)_i$ of a diffraction grating, that from now on we write in a more compact form as $(p_l)_i$; $l \in [1 \dots 5]$. On the other hand, y_i is a vector whose components are the CIE $L^*a^*b^*$ chromatic coordinates associated to each grating belonging to X . The CIE $L^*a^*b^*$ space is a perceptually uniform color space particularly suited to human perception [23].

The meta-model can thus be interpreted as an approximation of the non trivial relationship, noted $y_i = f(x_i)$, between the geometry of the grating and the color it generates. Mathematically, the meta-model can be written as

$$\begin{aligned} \tilde{f} : \mathbb{R}^5 &\rightarrow \mathbb{R}^3 \quad [\text{CIE } L^*a^*b^*]; \\ \tilde{y}_i &= \tilde{f}(x_i); \quad i = 1..N; \end{aligned} \quad (3)$$

which, in continuity with our previous work [12], was obtained using an artificial neural network (ANN) as intensive learning meta-model [24,25]. In this contribution we consider three hidden layers with 100 neurons each. The weights are determined through the minimization of the mean square error on the training set and the learning method employed is the gradient descent, which is calculated by the back-propagation principle.

To train the meta-model we generated a color database, composed of 14000 elements, using the spectra numerically obtained with the C-method, considering TM-polarized light and zeroth

order diffraction in reflection configuration. Throughout our numerical experiments we found that this size of the database was enough to minimize the average prediction error and, at the same time, to have a sufficient number of elements to generate the database in a reasonable time. Each geometrical parameter $(p_l)_{l=1..5}$ lies within the lower and upper bounds shown in Table 1. These values were chosen taking into account industrial feasibility considerations.

Table 1. Upper and lower bounds of each parameter used to generate the database.

parameter	lower bound	upper bound
$p_1 (R_\alpha)$	0.2	0.9
$p_2 (\Lambda)$	230nm	310nm
$p_3 (h)$	40nm	120nm
$p_4 (e\Lambda)$	5nm	35nm
$p_5 (eS)$	0nm	135nm

The chromatic response of each structure in the database was calculated using the CIE 2deg color matching functions and the standard illuminant D65. The related perceived colors are depicted in Fig. 4 in the CIE $L^*a^*b^*$ space. We can notice that by adjusting the structure's parameters, we can reach a wide and vivid visible color gamut.

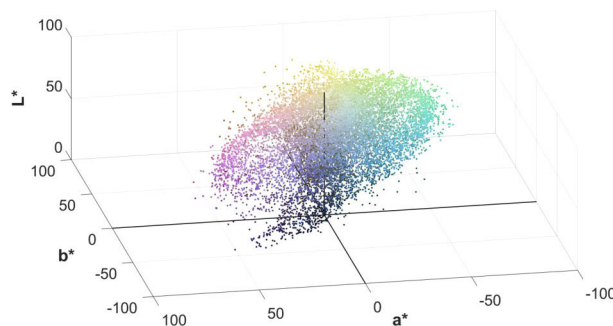


Fig. 4. Color data base obtained with electromagnetic simulations and shown in CIE $L^*a^*b^*$ space.

The difference between the initial color database and the predicted one is shown in Fig. 5(a). We quantify the prediction error through the color difference $\Delta E_{f,\tilde{f}} = \Delta E(f(x_i), \tilde{f}(x_i))$ with the formula given by CIEDE2000 [26]. The histogram in Fig. 5(b) illustrates the performance of the

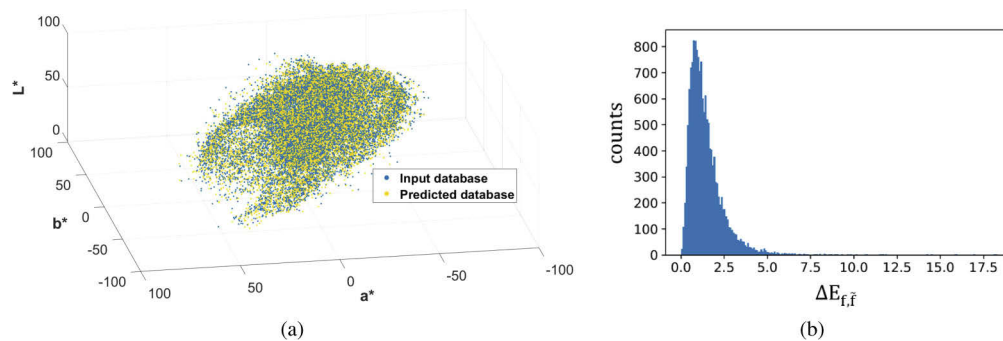


Fig. 5. (a) Difference in the CIE $L^*a^*b^*$ space between the initial color database and the predicted one using the trained ANN; (b) Histogram of color difference $\Delta E_{f,\tilde{f}}$ between the initial database and the predicted one.

meta-model prediction, we notice that 78% of the initial elements of the database are predicted with a $\Delta E_{f,\bar{f}} < 2$ and more than 98% with a $\Delta E_{f,\bar{f}} \leq 4$, a difference that is barely perceptible to the human eye. This result provides confidence on the accuracy of the meta-model and its use to replace the C-Method.

3. Inverse problem: color reproduction

In some applications where the goal is to generate true color images like, for example, in displays technologies or zero order devices (ZOD) for hologram security authentication images, a convenient approach often used is to define the requested colors and then to design the optimal structure that produces them (inverse problem). In this study, we aim at finding the optimal geometrical parameters of a structure, composed of three adjacent V-groove gratings, to best match the target color pixels labelled A, B and C in Fig. 6.

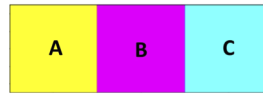


Fig. 6. Target colors.

An important fabrication constraint is that the three gratings must be simultaneously optimized on the same structure. Although each of them may have different geometrical parameters, they must share the same thicknesses of deposited materials, Al and Si_3N_4 in the present work. The reason for this restriction is that during the fabrication process it is easier to deposit one or several uniform layers all over the sample, for example by thermal evaporation, than layers of different thicknesses.

Very often, this kind of V-shape gratings is fabricated through the replication of a pattern into a polymer film. The hard master stamp (rigid mold) can be manufactured, for example, by focused ion beam (FIB) milling process [27] or by the combination of photolithography with anisotropic etching [28]. During the replication process, the transfer of the master pattern to the polymer film can be done by roll to roll or UV casting nano-imprint methods [29].

An optimal structure, noted s_k , should then be composed of the combination of three adjacent gratings $[x_A, x_B, x_C]_k$, each of them characterized by 5 geometrical parameters $[p_{1j}, p_{2j}, p_{3j}, p_4, p_5]_k; j = A, B, C$ as shown in Table 2, subject to the constraints

$$\begin{cases} p_{4A} = p_{4B} = p_{4C} = p_4 \\ p_{5A} = p_{5B} = p_{5C} = p_5 \end{cases} \quad (4)$$

Table 2. Definition of a structure composed of three pixels A,B,C sharing the fourth and fifth parameters.

	pixel A	pixel B	pixel C
R_α	p_{1A}	p_{1B}	p_{1C}
Λ	p_{2A}	p_{2B}	p_{2C}
h	p_{3A}	p_{3B}	p_{3C}
e_A		p_4	
e_S		p_5	

In order to relate the geometrical parameters of a grating with the searched color, we defined the objective functions g_A , g_B and g_C in terms of the CIE2000 color difference formula [26]

$$g_i = \Delta E(\text{TargetPixel}_i, \tilde{f}(x_i))_{i=A,B,C} \quad (5)$$

These objective functions measure the closeness between each target color A,B or C and each pixel's color computed with the meta-model. At first sight, one may intuitively think to formulate this multi-objective optimization problem as a mono-objective one to search for a single optimized solution, based on a weighted combination of all the objectives. Another more rigorous approach would be to take into account the different objective functions g_A , g_B and g_C making use of a dedicated multi-objective optimization method.

It should be noted that the presence of multiple objectives in a problem gives rise, in principle, to a set of optimal trade-off solutions (known as Pareto-optimal solutions) instead of a single optimal solution. The Pareto front fully determines the whole set of potential choices that optimally satisfy the trade-offs among the different objective functions. Basically, in a multi-objective optimization scheme each structure s_i is ranked by non-domination relationships based on its performance $(g_A, g_B, g_C)_{s_i}$. In our case, it was established that a structure s_1 dominates a structure s_2 if $g_i(s_1) \leq g_i(s_2)$; $i = A, B, C$ and $g_i(s_1) < g_i(s_2)$ for at least one function g_i . In the absence of any further information, one of these Pareto-optimal solutions cannot be said to be better than the others. In this case, a further processing is required to arrive at a single preferred solution. In general, from the set of optimal structures, one can select the solution that best fits the current design needs or provides insightful information on the physical phenomenon studied.

4. Results

At this stage it is convenient to illustrate the performance of our meta-model-based MOO scheme through some examples.

4.1. Limits of the mono-objective optimization

Let us define the objective functional h_1 to be minimized as

$$h_1 = \min(g_A + g_B + g_C) \quad (6)$$

where g_A , g_B and g_C are the color differences described in Sect. 3. Although, for the sake of brevity we only present in Fig. 7 some typical results obtained when Eq. (6) is minimized. The optimal geometrical parameters are retrieved with a numerical precision of 0.1 nm. Although this resolution is hardly reachable during the fabrication, the results of extensive numerical experiments showed that neither the spectra nor the colors are significantly modified at this scale. It should be noted that any other combination of these functions could be used as well. However, we found throughout our numerical simulations that the optimization algorithm, which was the Particle Swarm Optimization (PSO) [30] coupled with the meta-model presented earlier, converged to similar results. That is, the convergence strongly depends on the form of the functional chosen and the colors reproduced are far from the target ones, as it can be seen in Fig. 7 for the color pixel B. We used the PSO and ANN numerical implementations respectively provided by Python through the libraries PySwarm and Keras [31,32].

4.2. Meta-model based optimization scheme (MOMmBO)

As mentioned in Section 3, one way to avoid the situation illustrated by the previous example is to use multi-objective optimization, where the objective functions constitute a multi-dimensional space. Our goal thus is to retrieve the geometrical parameters of the structure in Fig. 1 that produce the target colors depicted in Fig. 6. That is, we aim at finding a trade-off among the objective functions g_A , g_B and g_C to be minimized (Section 3), subject to the constraints given



	Pixel A	Pixel B	Pixel C
R_α	0.82	0.46	0.44
Λ	258 nm	270.4nm	302.7nm
h	60nm	118.5nm	97.5nm
e_A	21.2 nm		
e_S	5.4 nm		

Fig. 7. Optimal solution obtained by minimizing the objective functional h_1 defined in Eq.(6).

by Eq. (4) and set to guarantee physical feasibility. Also, the upper and lower bounds of the searched geometrical parameters are shown in Table 1.

To search for the trade-off solutions, we used the Non-Dominated Sorting Genetic Algorithm (NSGA-II) for MOO [33], combined with meta-model described in Section 2. The NSGA-II is one of the most popular population-based algorithms used for evolutionary multi-objective optimization (EMO). It is a very efficient method for solving problems with a small number of objective functions. We used the implementation of NSGA-II provided in Python via the library Platypus [34] with 1000 initial individuals and 50000 iterations, the optimal 3D-Pareto front obtained is shown in Fig. 8(a).

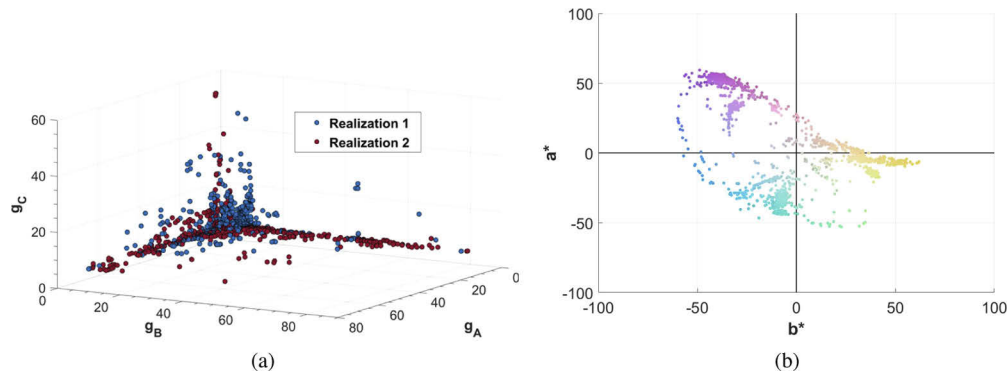


Fig. 8. (a) 3D Pareto-fronts obtained by minimizing (g_A, g_B, g_C) , two realizations with different initial random population are reported; (b) 3D-Pareto front shown in the projected a^*b^* plane.

In order to assess the convergence behavior of the NSGA-II, we searched for the target colors in Fig. 6 considering different randomly generated initial populations. To facilitate the visualization, we show in Fig. 8(a) only two of the 3D-Pareto fronts obtained. This result suggests that the NSGA-II is not sensitive to initialization and presents a good reproducibility. Furthermore, despite the large number of evaluations needed because of the population size, the meta-model \tilde{f} makes possible to obtain a 3D-Pareto front in about 311 seconds.

We see that there are off-center solutions which favor two objective functions while giving poor performances to the third one. Nevertheless, at this stage, the solutions that will be retained will be mainly those which minimize the three functions simultaneously as $g_A, g_B, g_C < 30$. We display in Fig. 8(b), using the projected CIE a^*b^* plane space, the 1000 solutions obtained in the 3D-Pareto front. We see that the resulting front does not give completely aberrant solutions, as these remain about potentially acceptable colors.

In Fig. 9(a), we show an example of solution found in the Pareto front obtained with $g_A = 13.02$, $g_B = 11.42$ and $g_C = 9.76$ with the corresponding specular reflexion spectra in Fig. 9(b).

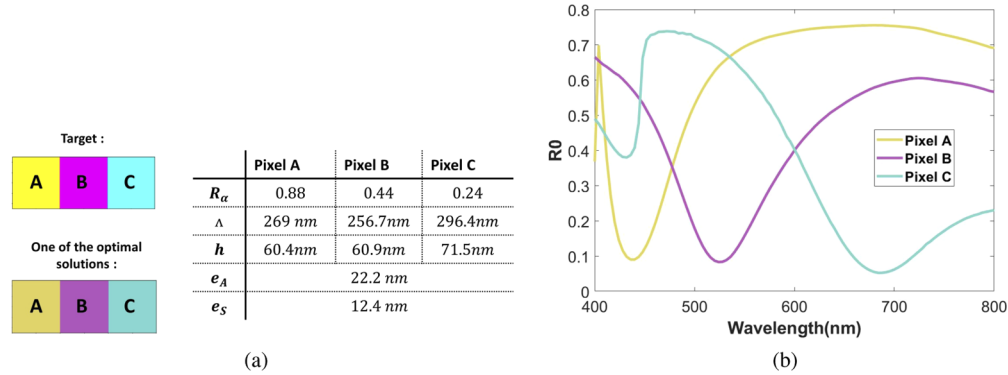


Fig. 9. (a) One of the solutions found on the 3D Pareto-front obtained with $g_A = 13.02$, $g_B = 11.42$, $g_C = 9.76$; (b) Reflexion spectra of the optimal structure presented in Fig. 9(a).

The retrieved colors are by far closer to the target ones than those depicted in Fig. 7 obtained using the mono-objective optimization.

4.3. Robustness

An important issue in our study is to obtain robust solutions insensitive to the variations of the design variables, which correspond to the potential error introduced when the samples are fabricated. To identify the most robust solutions, noted s_k^* , among those located in the Pareto front, we defined a 5-dimensional hyper volume centered on s_k^* and with a radius of ϵ , where $\pm\epsilon$ is the accuracy of the fabrication process. In our case, we fixed arbitrarily $\epsilon = [0.025, 2nm, 2nm, 2nm, 2nm]$. This parameter is to be adjusted according to the estimated accuracy of the used manufacturing technology.

In this hyper-volume, we chose randomly M elements s_{kl}^* ; $k = 1..P$ and $l = 1..M$, where P and M respectively represent the number of Pareto optimal solutions and the number of robustness testing points about each solution of the Pareto set. In our case, $P = 1000$ corresponded to the population size chosen for the optimization process and M was arbitrarily fixed to 500. We then calculated the predicted colors $\tilde{f}(s_{kl}^*)$ using the meta-model.

A robust solution s_k^* will be therefore a solution with a small color difference $Dv_{kl} = \Delta E(\tilde{f}(s_{kl}^*), \tilde{f}(s_k^*)); \forall l \in 1..M$ with respect to each structure within the hyper-volume.

Each individual s_{kl}^* within the hyper-volume was then ranked based on its performance Dv_{kl} . We chose then to analyse the distribution of individual performances by calculating the mean of the best and the worst ranked elements. This analysis guarantees that during the fabrication process, independently of where the error is between $\pm\epsilon$, even in the worst configuration, the color will not change significantly. We show in Fig. 10 (yellow dots), the most robust optimal solutions. It remains to choose from this set the easiest solution to manufacture.

Before closing this section we emphasize, once again, the importance of the meta-model on the significant reduction of the computing time required in the robustness study.

This can be better visualized computing the number of required electromagnetic simulations, which is given by the product $P \times M$, where P and M are the parameters previously defined. Since the estimated time required for one simulation is about 42 s and $P \times M = 500000$ simulations, one easily finds that 243 days would be necessary to perform all the numerical simulations. It is important to notice that, at least for the present application, these computing times were enough

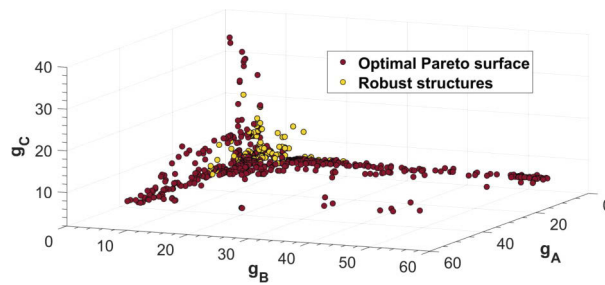


Fig. 10. Optimal 3D-Pareto front (red points) and robust optimal solutions (yellow dots).

to obtain the expected results. However, this should not be necessarily the case for problems in which a larger number of iterations may be required.

4.4. Pareto solutions analysis

The set of optimal solutions is used not only to achieve an optimal design, but also to obtain and extract additional information to better understand how the geometrical parameters affect the observed spectral variations. It also serves as a guide to understand the physical phenomena underlying the generation of colors.

We show in Fig. 11 the distribution of the optimal geometrical parameters $p_{l=1..3}$ obtained on the Pareto front for fixed values of the thickness e_A and e_S . We see in Fig. 11(a) and Fig. 11(b) that, even though it depends on the period Λ and the amplitude h , R_α seems to be the geometrical parameter that introduces the most significant spectral differences between the three pixels. That is, for example, two structures belonging to the 3D-Pareto front can have the same period ($\Lambda = 265\text{nm}$ for example) but two different colors (pixel A and B) if the parameter R_α is different (Fig. 11(a)). Furthermore, the grating depth h does not vary drastically between the three pixels (Fig. 11(b)). Thus, at constant h and Λ , different colors can be obtained just by modifying the groove angle.

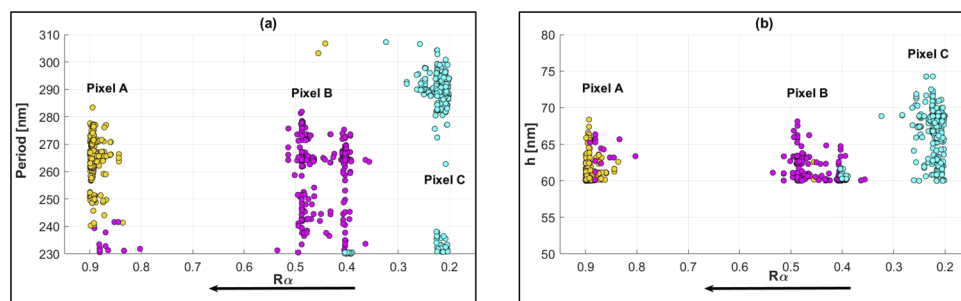


Fig. 11. Parameters distribution (R_α , Λ , h) of the optimal structures of each pixel obtained on the Pareto front.

This fact suggests that the angle of the V-groove governs the origin of the spectral variations observed between the three pixels. It has been shown that gap surface modes (GSPs) confined laterally between the tapered groove sidewalls can be excited in such structures. As it can be seen in Fig. 12, where near-field intensity maps have been computed for resonance wavelengths of the three optimal pixels' structures presented in Fig. 9(b), there is a strong field confinement in the z direction especially when decreasing the groove's angle (Fig. 12(c)). The tapered groove can be seen as a stack of infinitesimally thick metal-insulator-metal structure, with a variable

insulator thickness along the z direction. Then, the lower the thickness, the more the effective refractive index and the confinement of the field are important [35,36]. However, if the V-groove angle is large, these GSPs modes can leak into surface plasmons on the side of the groove. It has been previously shown, for the case of V-grooves milled in a semi infinite metallic surface, that these resonant peaks are related to the formation of standing waves due to interference of counter propagating GSPs reflected by the groove bottom and opening [37,38]. Nevertheless, further studies are needed for the case of hybrid thin films as the ones considered in this contribution. However, this is out of the scope of the present work and it will be subject of a future publication.

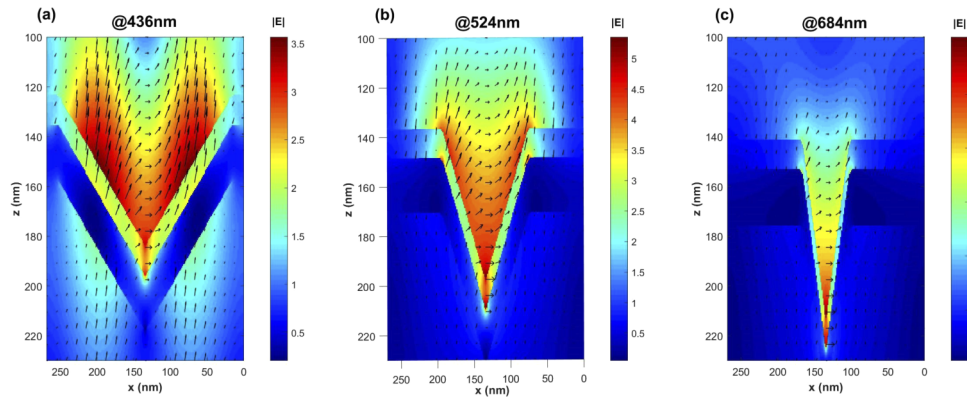


Fig. 12. Time averaged (colormap) and displacement (black arrows) of the electric field at resonance wavelengths (a),(b),(c) of respectively the pixels A,B and C of the optimal structure presented in Fig. 9(a).

5. Concluding remarks

The research evidence presented in this contribution clearly shows that the use of modern optimization tools, prior to fabrication, provides an efficient way to tailor and to optimize the optical or resonant response of an optical device for a particular application. In this sense, within the frame of the present work, the use of a multi-objective approach, which clearly outperforms mono-objective strategies, opens the possibility to increase the complexity of the diffractive structures employed for color reproduction, thus leading to chromatic effects useful for the design of optically variable devices like those used for optical documents security, to give an example.

In the present work, a post-optimization study served to find those optimized diffraction gratings less sensitive to variations of the geometrical parameters, which is an unavoidable situation when the structure is fabricated even with modern laboratory equipment. Furthermore, the post-optimization stage made evident that among the geometrical parameters optimized, the groove's angle of aperture had the strongest effect on the generation of color.

The inclusion of a meta-model in the optimization process is a practical way to significantly decrease the computing time. As it has been shown throughout this work, the iterative nature of the multi-objective approach makes the optimization of the diffraction gratings extremely long when done with the rigorous electromagnetic method. It should be noted that generating the database to train and validate the neural network can be time consuming; however, this is done just once. Afterwards, the meta-model can be used without being necessarily included in an optimization process.

At last, the modular structure of the optimization scheme presented in this work not only facilitates its numerical implementation, but it also makes of it a generic and suitable tool that could be easily used for the solution of inverse or optimization problems in other branches of optics and photonics.

Funding

Agence Nationale de la Recherche (ANR-16-CE39-0016-01, ANR-14-LAB5-0007).

References

1. Y. Gu, L. Zhang, J. K. W. Yang, S. P. Yeo, and C.-W. Qiu, "Color generation via subwavelength plasmonic nanostructures," *Nanoscale* **7**(15), 6409–6419 (2015).
2. T. Lee, J. Jang, H. Jeong, and J. Rho, "Plasmonic- and dielectric-based structural coloring: from fundamentals to practical applications," *Nano Convergence* **5**(1), 1 (2018).
3. C. Yang, W. Shen, Y. Zhang, H. Peng, X. Zhang, and X. Liu, "Design and simulation of omnidirectional reflective color filters based on metal-dielectric-metal structure," *Opt. Express* **22**(9), 11384–11391 (2014).
4. K. Kumar, H. Duan, R. S. Hegde, S. C. W. Koh, J. N. Wei, and J. K. W. Yang, "Printing colour at the optical diffraction limit," *Nat. Nanotechnol.* **7**(9), 557–561 (2012).
5. A. S. Roberts, A. Pors, O. Albrektsen, and S. I. Bozhevolnyi, "Subwavelength plasmonic color printing protected for ambient use," *Nano Lett.* **14**(2), 783–787 (2014).
6. S. J. Tan, L. Zhang, D. Zhu, X. M. Goh, Y. M. Wang, K. Kumar, C.-W. Qiu, and J. K. W. Yang, "Plasmonic color palettes for photorealistic printing with aluminum nanostructures," *Nano Lett.* **14**(7), 4023–4029 (2014).
7. A. K. González-Alcalde, R. Salas-Montiel, H. Mohamad, A. Morand, S. Blaize, and D. Macías, "Optimization of all-dielectric structures for color generation," *Appl. Opt.* **57**(14), 3959–3967 (2018).
8. C. Yang, L. Hong, W. Shen, Y. Zhang, X. Liu, and H. Zhen, "Design of reflective color filters with high angular tolerance by particle swarm optimization method," *Opt. Express* **21**(8), 9315–9323 (2013).
9. P. R. Wiecha, A. Arbouet, C. Girard, A. Lecestre, G. Larriou, and V. Paillard, "Evolutionary multi-objective optimization of colour pixels based on dielectric nanoantennas," *Nat. Nanotechnol.* **12**(2), 163–169 (2017).
10. J. Jung, "Robust design of plasmonic waveguide using gradient index and multiobjective optimization," *IEEE Photonics Technol. Lett.* **28**(7), 756–758 (2016).
11. K. Yao, R. Unni, and Y. Zheng, "Intelligent nanophotonics: merging photonics and artificial intelligence at the nanoscale," *Nanophotonics* **8**(3), 339–366 (2019).
12. V. Kalt, A. K. González-Alcalde, S. Es-Saidi, R. Salas-Montiel, S. Blaize, and D. Macías, "Metamodeling of high-contrast-index gratings for color reproduction," *J. Opt. Soc. Am. A* **36**(1), 79–88 (2019).
13. K.-Y. Kim and J. Jung, "Multiobjective optimization for a plasmonic nanoslit array sensor using kriging models," *Appl. Opt.* **56**(21), 5838–5843 (2017).
14. D. Liu, Y. Tan, E. Khoram, and Z. Yu, "Training deep neural networks for the inverse design of nanophotonic structures," *ACS Photonics* **5**(4), 1365–1369 (2018).
15. I. Malkiel, A. Nagler, M. Mrejen, U. Arieli, L. Wolf, and H. Suchowski, "Deep learning for design and retrieval of nano-photon structures," arXiv:1702.07949 [physics] (2017).
16. I. Sajedian, T. Badloe, and J. Rho, "Optimisation of colour generation from dielectric nanostructures using reinforcement learning," *Opt. Express* **27**(4), 5874–5883 (2019).
17. "Modal and c methods grating software <https://mcgrating.com/>,"
18. J. Chandezon, G. Raoult, and D. Maystre, "A new theoretical method for diffraction gratings and its numerical application," *J. Opt.* **11**(4), 235–241 (1980).
19. L. Li, J. Chandezon, G. Granet, and J.-P. Plumey, "Rigorous and efficient grating-analysis method made easy for optical engineers," *Appl. Opt.* **38**(2), 304–313 (1999).
20. M. G. Moharam and T. K. Gaylord, "Rigorous coupled-wave analysis of planar-grating diffraction," *J. Opt. Soc. Am.* **71**(7), 811–818 (1981).
21. L. Li, "Multilayer-coated diffraction gratings: differential method of chandezon et al revisited," *J. Opt. Soc. Am. A* **11**(11), 2816 (1994).
22. Y. Mei, H. Liu, and Y. Zhong, "Treatment of nonconvergence of fourier modal method arising from irregular field singularities at lossless metal-dielectric right-angle edges," *J. Opt. Soc. Am. A* **31**(4), 900–906 (2014).
23. J. Schanda, ed., *Colorimetry: understanding the CIE system* (Wiley, Hoboken, NJ, 2007). OCLC: 255647975.
24. I. Goodfellow, Y. Bengio, and A. Courville, *Deep learning*, Adaptive computation and machine learning (The MIT Press, 2016). OCLC: 955778308.
25. R. R. Barton and M. Meckesheimer, "Chapter 18 metamodel-based simulation optimization," in *Handbooks in Operations Research and Management Science*, vol. 13 (Elsevier, 2006. pp. 535–574.
26. M. R. Luo, G. Cui, and B. Rigg, "The development of the cie 2000 colour-difference formula: Ciede2000," *Color Res. Appl.* **26**(5), 340–350 (2001).
27. W. Wang, D. Rosenmann, D. A. Czaplewski, X. Yang, and J. Gao, "Realizing structural color generation with aluminum plasmonic v-groove metasurfaces," *Opt. Express* **25**(17), 20454–20465 (2017).
28. M. J. Madou, *Fundamentals of Microfabrication: The Science of Miniaturization, Second Edition* (CRC Press, 2002), 2nd ed.
29. I. Fernandez-Cuesta, R. B. Nielsen, A. Boltasseva, X. Borrísé, F. Pérez-Murano, and A. Kristensen, "V-groove plasmonic waveguides fabricated by nanoimprint lithography," *J. Vac. Sci. Technol., B: Microelectron. Nanometer Struct.–Process., Meas., Phenom.* **25**(6), 2649–2653 (2007).

30. J. Robinson and Y. Rahmat-Samii, "Particle swarm optimization in electromagnetics," *IEEE Trans. Antennas Propag.* **52**(2), 397–407 (2004).
31. "Particle swarm optimization (PSO) with constraint support pyswarm 0.6 documentation <https://pythonhosted.org/pyswarm/>,".
32. "Keras documentation <https://keras.io/>,".
33. K. Deb, A. Pratap, S. Agarwal, and T. Meyarivan, "A fast and elitist multiobjective genetic algorithm: Nsga-ii," *IEEE Trans. Antennas Propag.* **6**(2), 182–197 (2002).
34. "Getting started platypus documentation,".
35. C. L. C. Smith, N. Stenger, A. Kristensen, N. A. Mortensen, and S. I. Bozhevolnyi, "Gap and channeled plasmons in tapered grooves: a review," *Nanoscale* **7**(21), 9355–9386 (2015).
36. Y. Kurokawa and H. T. Miyazaki, "Metal-insulator-metal plasmon nanocavities: Analysis of optical properties," *Phys. Rev. B* **75**(3), 035411 (2007).
37. T. Søndergaard, S. I. Bozhevolnyi, J. Beermann, S. M. Novikov, E. Devaux, and T. W. Ebbesen, "Resonant plasmon nanofocusing by closed tapered gaps," *Nano Lett.* **10**(1), 291–295 (2010).
38. T. Søndergaard and S. I. Bozhevolnyi, "Surface-plasmon polariton resonances in triangular-groove metal gratings," *Phys. Rev. B* **80**(19), 195407 (2009).